

EXPERIMENTAL STUDY AND NUMERICAL MODELING OF NATURAL CONVECTION WITH CONDENSATION

Kaushik Das,¹ Randall Fedors,² Chandrika Manepally,¹ and Debashis Basu¹

¹Center for Nuclear Waste Regulatory Analyses
Southwest Research Institute®
San Antonio, TX

²U.S. Nuclear Regulatory Commission
Washington, DC

Contact: K. Das, kdas@swri.org, Telephone: +1-210-522-4269

Two-phase convective heat and mass transfer processes in a thermally perturbed, gas-phase dominant environment are studied using an experimental technique and numerical models. The broad objective of the study is to better understand the interplay of these processes and to improve the capability to simulate moisture redistribution in thermally perturbed environments utilizing a computational fluid dynamics (CFD) code. High-level radioactive waste emplacement in an underground facility is a projected scenario leading to thermal perturbations. Decay heat load from spent nuclear fuel and available liquid water at the repository wall could lead to moisture redistribution, characterized by repeated condensation-evaporation cycles and driven by natural convection, commonly referred to as cold trap. In the present study, laboratory experiments were conducted to understand the basic condensation evaporation cycle and provide validation support for numerical modeling to simulate heat transfer processes in concert with moisture redistribution. Within a rectangular enclosure, evaporation from a heated water source and condensation rate on a cooled wall were measured for a range of temperatures. The air temperature was monitored at specific locations inside the domain. A numerical model was constructed to study the natural convection and phase change using a species transport and multiphase mixture model in the CFD package ANSYS-FLUENT-12.1. Results of the comparison between measured and simulated temperature and condensation rates are presented; these show reasonable agreement between the predicted and experimental data. The present study also describes two different equilibrium models used to calculate saturation level in the fluid and their effect on computed results.

I. INTRODUCTION

Convective heat and mass transfer in thermally perturbed, dominantly gas-phase environments becomes difficult to assess in geometrically complex volumes. Use of validated CFD codes for geometrically complex problems is generally the preferred approach in capturing the flow and thermal field. Radiative, convective, and conductive heat transfer could all affect temperature distributions. In addition, the latent heat infusion into the flow field due to the combined evaporation-condensation cycle at the wall boundary and the volumetric flow field also changes temperature patterns. Essentially, the heat and mass transfer processes affect each other in an interactive manner where the evaporation, transport, and condensation depend on the natural convection pattern and overall heat transfer is dependent on the phase change rate. The repeated condensation-evaporation cycle and natural convection are encountered in a number of applications related to high-level waste disposal in unsaturated zone, especially in the cold trap process. In this process, seepage water evaporates due to radioactive decay heat and condenses on relatively cooler surfaces causing water redistribution in underground openings. Similar physical processes also take place in condensers and nuclear power plant components.

Resolving the conjugate heat and mass transfers in a general purpose CFD code requires a modeling capability that solves the species transport equations in addition to the continuous flow field in a multiphase environment. The solver also must (i) address the issue of phase change at the wall and the continuous flow field and (ii) track the condensate liquid mass that accumulates due to volumetric phase change. The commercial CFD package ANSYS-FLUENT-12.1¹ has been adopted to

study this coupled multiphase heat and mass transfer process. The solver has a multiphase flow framework which was used along with a species transport module that enabled simulation of evaporation, vapor transport, and condensation. User-defined functions were developed and added to address the issue of film condensation at the wall and volumetric condensation in the flow field.

Detailed laboratory tests were conducted to verify the overall modeling capabilities of the general purpose solver in predicting the flow and thermal field. This well-constrained, small-scale laboratory model was also meant to validate the added user-defined modules for calculating the wall and volumetric evaporation-condensation process before future modeling of a large-scale experiment with complex geometry. The experiment was conducted to obtain measurements of water transport rates in a simple two-dimensional natural convection flow. To simplify the validation experiment, low temperatures and temperature gradients were used so that radiation could be neglected. The present study will first describe the small-scale experiment and measurement results for temperature distribution and condensate rate. Subsequently, the numerical model development process will be described and results from this analysis will highlight the comparison between the measured water transport rates and the rates predicted by the CFD model.

II. DESCRIPTION OF WATER TRANSPORT EXPERIMENTS

Laboratory tests were conducted to measure the amount of water transported from a heated water source to a cold (condensation) plate. Multiple tests were conducted by varying the heat rate to the water source and varying the temperature of the cold plate. Once steady-state temperatures were attained for a test, water transport rates were determined by measuring condensation draining from the cold plate. The test chamber is described next.

II.A. Test Chamber

A schematic diagram and photographs of the test chamber are shown in Fig. 1. The enclosure was made of polycarbonate sheet, acrylic sheet, and aluminum. Water evaporated from the heated tray shown on the bottom left of the enclosure. Water was continuously added to the water tray to maintain the level. Water was condensed on the cooled aluminum plate shown on the right side of the test enclosure. This condensate flow was collected in a graduated cylinder and the rate of collection was recorded.

The chamber was 23 inches [0.58 m] long, 6 inches [0.15 m] tall, and 12 inches [0.30 m] wide. The tray holding the source water was 3 inches [0.08 m] long and ran the entire width of the chamber. The top wall of the chamber was made from 1-inch-thick acrylic. The left end wall and bottom wall (except for the water tray, which was made of aluminum) were made of 1-inch-thick [0.03 m] polycarbonate. The front and back walls of the chamber were made of 0.5-inch-thick [0.01 m] polycarbonate. The cold plate was made of 1-inch-thick [0.03 m] aluminum and channels were drilled through it so cooling fluid could circulate through the plate. Though not shown in Fig. 1, the entire chamber was covered with a 1-inch-thick [0.03 m], and later a 2-inch-thick [0.06 m] shell of polystyrene foam insulation to reduce heat loss. The chamber sat on a table on top of two sheets of polystyrene foam insulation.

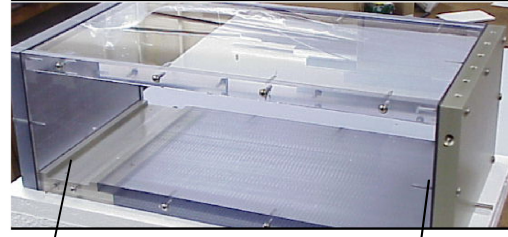
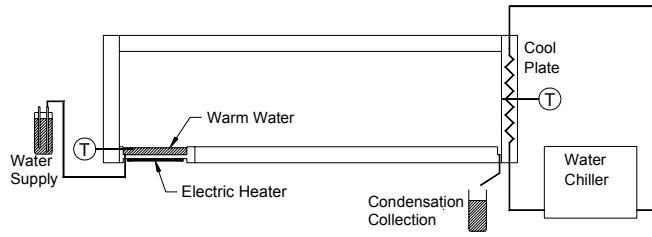
The water was warmed by an electric heater bonded directly to the bottom of the aluminum water tray. The heater pad was the same dimensions as the water tray. The heater pad was powered by a variable AC supply so that the power level could be varied. Based on the design of heating and cooling components, a two-dimensional convection cell was expected to form in the plane following the length and height of the chamber; temperature measurements were made at the centerline of the width.

Thermocouples were installed in the test chamber to measure the evaporator, condenser, and air temperatures. The locations of the temperature sensors in the test chamber are shown in Fig. 2. The thermocouples were Omega, Type K, model number 5TC TT K 30 72 with a bare wire junction and 0.01-inch-diameter wire. A calibration check showed that all of the temperature sensors were within 0.2 °C of the standard thermometer reading.

Water that drained off of the cold plate was collected and measured in a graduated cylinder. Depending upon the condensation rate and collection time, different sized graduated cylinders were used to collect the fluid to improve measurement resolution.

II.B. Observations and Test Measurements

Several tests were conducted to measure the moisture transport rate from the water tray at one end of the chamber to the cold plate at the other end of the chamber. For each heat rate and cold plate temperature, the rate of water condensing at the cold plate was recorded after steady-state temperatures were reached. The test results are shown in Table I. The values given in Table I are averages measured over several hours after steady-state temperatures



(a)

(b)

Fig. 1. (a) Side view schematic of laboratory test chamber and (b) photographs of the chamber; entire chamber and close-up view of source water reservoir

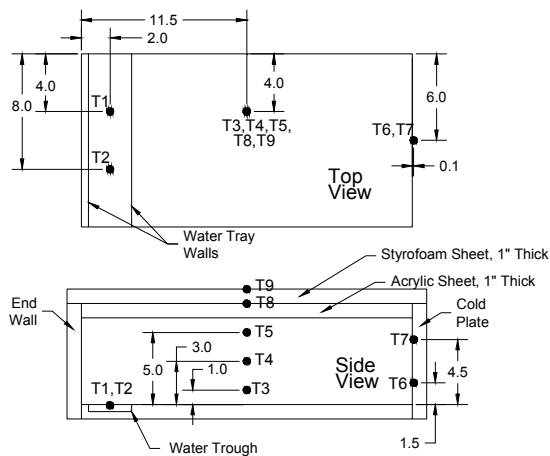


Fig. 2. Temperature sensor locations and dimensions of the chamber (top and side views)

were reached. Data from Tests 4–15 in Table I is summarized in Fig. 3 where the variation of the condensation rate is plotted as a function of the temperature difference between the source water and the cooled condensation wall. Three temperature curves (tagged as 5, 20, and 30 °C) used in the experiment represent different convection regimes. Fig. 3 shows that condensation increases both with temperature difference (hot source water minus cold condensation plate) and with a different convection regime.

Light condensation forming was observed on the inside surface of the chamber along the top wall and the sidewalls after the initial set of tests (Tests 1–3). The condensation on the top wall started about 12 inches from the cold plate. The amount of condensate on the top wall increased (larger diameter drops) closer to the cold plate. The condensation on the sidewalls near the top also started about 12 inches from the cold plate. The amount of condensate on the

side walls increased closer to the cold plate. The condensation on the sidewalls did not reach all the way to the bottom of the chamber; the bottom couple of inches had no condensation. It was anticipated that the heat loss through sidewalls caused condensation formation on the sidewalls in Tests 1–3. An analysis of the energy balance was performed considering the heater power and the heat loss to the ambient environment. The heat loss through the insulation was estimated using the insulation thickness, chamber surface area, insulation thermal conductivity (0.026 W/m K), and the temperature difference measured across the insulation on the top of the chamber.

The amount of water that could be condensed in the chamber from the heat lost to the ambient temperature can be estimated from the heat loss rate and the heat of vaporization for water (0.63 W hr/g at 100 °C). The heat loss rate estimated for Test 3 was 5.4 W, which corresponds to a condensation rate of 8.6 ml/hr of water. For this test, the measured condensation rate was 25.6 ml/hr, so the ambient losses are significant. Note that this simplified analysis does not consider any cooling of the water or air in the chamber and assumes all heat lost to ambient temperature becomes condensation. To reduce the heat losses after Test 3, the shell of insulation surrounding the test chamber was increased to a 2-inch thickness.

III. NUMERICAL MODELING OF THE MOISTURE TRANSPORT EXPERIMENTS

A numerical model was developed using the commercial CFD package ANSYS-FLUENT Version 12.1 to replicate the experimental study. It uses a control-volume-based technique to convert a general scalar transport equation to an algebraic

TABLE I. Test Results and Test Conditions. Temperature Sensor Locations T1–T9 Are Shown in Fig. 2.

Test No.	Condensation Rate (ml/hr)	Water Temp. (C)	Cold Plate Temp. (C)	Air Temp-Lower (C)	Air Temp-Middle (C)	Air Temp-Upper (C)	Temp. Top Chamber (C)	Temp. Top Insulation (C)
		T1,T2	T6,T7	T3	T4	T5	T8	T9
1	8.8	38.6	10.7	22.9	26.0	27.2	25.4	23.7
2	16.8	46.1	10.8	26.6	30.2	31.5	29.0	24.1
3	25.6	54.3	10.9	30.9	35.2	36.3	33.1	24.5
4	7.2	32.3	5.3	18.8	21.6	23.2	22.4	24.5
5	12.1	39.4	5.4	21.5	24.9	26.6	24.7	23.1
6	20.9	47.7	5.5	25.1	29.1	30.9	29.0	23.7
7	4.7	25.3	5.2	15.6	17.9	19.2	18.7	23.3
8	2.5	19.5	5.2	14.3	16.3	17.4	18.2	24.2
9	1.7	26.2	19.1	22.6	23.5	24.1	24.0	25.4
10	6.6	38.2	19.1	26.3	28.3	29.5	27.9	25.1
11	20.8	50.9	19.3	32.1	35.3	36.8	34.4	25.1
12	12.8	45.0	19.2	29.2	32.1	33.4	31.5	26.2
13	8.1	46.1	29.5	33.7	35.5	36.6	34.8	25.1
14	4.2	39.7	29.4	31.3	32.2	33.1	31.5	23.9
15	0.5	34.0	29.4	29.7	30.1	30.5	29.6	25.2
16	0.0	57.5	19.3	32.3	35.8	37.4	33.6	25.8
17	0.0	44.2	19.3	27.9	30.3	31.6	29.3	25.3
18	0.0	32.3	19.2	23.8	25.2	26.1	25.0	23.8

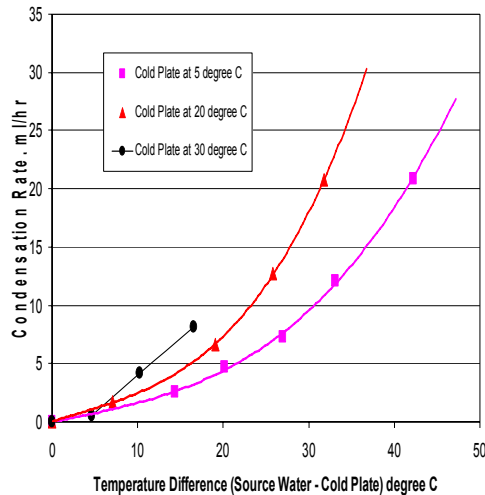


Fig. 3. Experimental results showing the change in the condensation rate as a function of the difference between the heated water and cold plate temperatures

equation that is solved numerically. A variety of spatial and temporal discretization schemes as well as turbulent models are also available in FLUENT. Simulation parameters were chosen to suit natural convection flows. For the present simulations, the pressure-based solver was chosen, as the flow can be considered to be in the incompressible fluid. The full three-dimensional Navier Stokes equations were solved using an unsteady, implicit approach. The Semi-Implicit Pressure Linked Equations–Consistent (SIMPLEC) algorithm² was used to treat pressure-velocity coupling for stability. The third order Monotone Upstream-Centered Schemes for Conservation Laws (MUSCL) were used to derive the face values of different variables for the spatial discretization, which were used to compute the convective fluxes. The Rhie-Chow scheme³ was selected to interpolate pressure at the control volume face and to satisfy the mass conservation without pressure oscillations. For simulating turbulence, the shear stress transport (SST) $k-\omega$ model⁴ was used.

III.A. Methodology

Three distinct mass transfer and transport processes can be identified in the experimental setup described in the previous section that need customized modeling techniques and boundary conditions not available in the standard version:

- (i) Mass transfer at the walls due to condensation and evaporation that is modeled using suitable boundary conditions
- (ii) Transport of evaporated water vapor from the hot source location to the cold wall due to buoyancy-driven natural convection
- (iii) Condensation of water vapor within the flow domain, where the temperature locally drops below the saturation point.

The third process would generate liquid water that will then be transported with the air and water vapor mixture. The quantity of condensed liquid water would be very small, and the fluid dynamic impact on the gas phase will be minimal. The thermodynamic effect, however, could be significant due to latent heat exchange between phases.

In the present study, the mass transfer process at the wall due to condensation and evaporation is modeled using a suitable boundary condition following a standard approach⁶. Local thermodynamic equilibrium is assumed to occur at the liquid-vapor interface, and the saturation condition was specified as boundaries. This approach also assumes only film condensation occurs; i.e., droplet condensation is excluded. Also, any phase change heat transfer takes place with the wall and does not affect the gas phase. Using these assumptions, the condensation rate can be calculated as the water vapor rate of diffusion toward the cold surface. This method of estimating condensation rate is reasonable because diffusion across boundary layers is the rate-limiting process. The mass, momentum, and energy equation source terms were calculated and implemented into the solver to account for the loss and gain of water vapor at the hot and cold boundaries.

The mixing and transport of the air water vapor mixture were modeled by solving the conservation equations for every species individually, within a phase. The number of phases depends on the way volumetric condensation is treated, which is described in the next section. A mixture template of air and water vapor was defined with respective material properties. An incompressible ideal gas approximation was used to calculate mixture density. The diffusion energy source for the species equations was considered, as diffusion might be significant in the low speed near-wall region. The direction of the

gravity vector and an operating pressure were specified to simulate buoyancy.

The issue of volumetric condensation in the domain was addressed using two different techniques. In the first technique, referred to as the nonequilibrium method, the effect of gas phase condensation was neglected and localized supersaturation of water vapor was allowed. The allowable limit was set based on the kinetic theory.⁵ Hence, for the nonequilibrium model, a single mixture phase is considered. In the second approximation, volumetric condensation was considered and is referred to as the equilibrium model. The maximum level of water vapor in the system was dictated by the saturation limit, and any moisture content above this limit would condense and form liquid water as a second phase in the system.^{6,7} The water droplets would form mist and move with the convecting flow, but coalescence and rainout of droplets were not considered in the model. The equilibrium mass transfer process was coded as a user-defined routine and added to the solver. For the equilibrium model, two different phases are modeled using the “mixture” multiphase flow model. In this model, the flow variables are obtained by solving the momentum, continuity, and energy equations for the mixture, and for the secondary liquid droplet phase, volume fraction equations are solved. Individual phase quantities are determined using algebraic expressions for the relative velocities.

III.B. Modeling Results

Fig. 4 highlights the computational domain and the boundary condition of the model. A total of 17,000 nodes are used for the calculation and the node size was determined using a separate grid independence study. Grids are clustered near the wall to capture flow, temperature, and concentration gradients. As discussed in the previous section, saturation condition was specified at the water source and the cold wall corresponding to the experimental temperature at those locations. The rest of the wall was assigned an adiabatic boundary condition as the heat transfer through those walls can be assumed to be negligible.

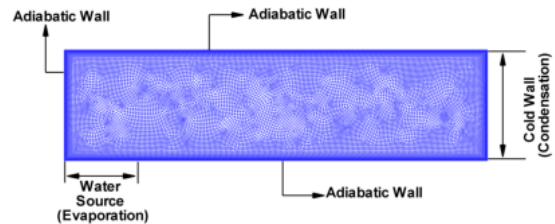


Fig. 4. Computational grid and boundary condition

Simulations were performed for conditions corresponding to Tests 1–14. The general flow and temperature field data discussed here for both the models correspond to Test No.-11 of Table I.

Figs. 5(a) and (b) show the velocity magnitude contours obtained using the nonequilibrium and equilibrium models, respectively. In general, a strong plume is generated from the hot water source that moves upward due to the density difference between the hot and the cold fluid. This plume reaches the upper wall and then moves toward the cold wall. Another high velocity region can be noticed near the cold wall, where the fluid undergoes mass transfer and the colder fluid flows back to the water source creating a cyclic convection pattern that encircles the whole domain. However, there is no noticeable difference between the two models, indicating that volumetric condensation has little impact on the velocity field.

Figs. 6(a) and 6(b) show the temperature field calculated using the equilibrium and nonequilibrium models. A high temperature zone can be identified near the hot water source and the temperature adjacent to the cold wall is lower than the rest of the domain. Though the temperature patterns predicted by both models are qualitatively similar, some difference in velocity magnitude can be noted near the bottom wall of the enclosure. The overall

temperature distribution is not greatly affected by volumetric condensate formation, though it can affect localized temperature distribution.

Figs. 7(a) and (b) illustrate the relative humidity contours of the nonequilibrium and equilibrium models. Note that a substantial part of the domain has relative humidity slightly above 100 percent for simulations that use the nonequilibrium model. This is because supersaturation was allowed in the domain and any possible mass transfer from the air water vapor mixture was not considered in calculation. The equilibrium model shows a different pattern of relative humidity distribution, where the maximum value is capped at 100 percent as any water vapor that contributes to supersaturation condenses to form liquid water. Though supersaturation does not normally occur in enclosed space, researchers^{8,9} have indicated that it can be attained under limited circumstances and the maximum level of supersaturation can be determined using the kinetic theory.

Fig. 8 shows the interphase volumetric mass transfer rate for the equilibrium model. The mass transfer rate is small and is only confined to a certain region near the hot water source and the cold wall. These regions correspond to high relative humidity zones obtained using the

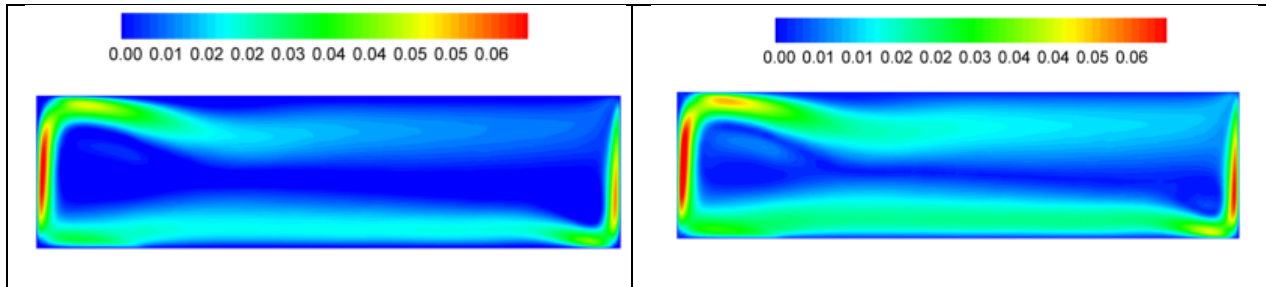


Fig. 5(a). Velocity (m/s) contours using non-equilibrium model (without volumetric condensation) and (b) velocity (m/s) contours using equilibrium model (with volumetric condensation)

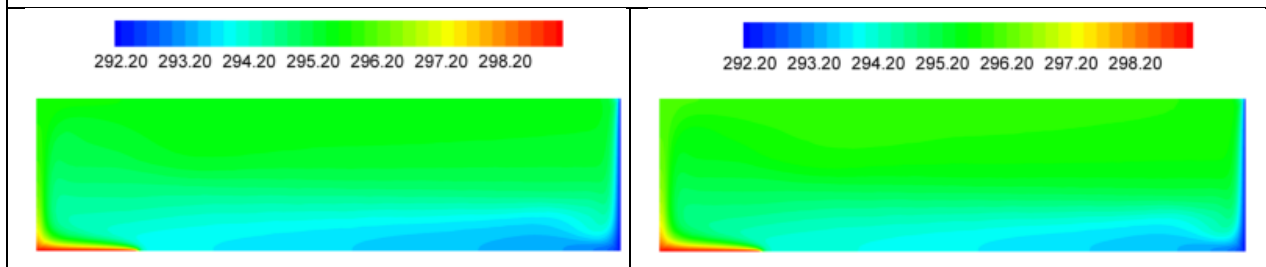


Fig. 6(a). Temperature (K) contours using nonequilibrium model (without volumetric condensation) and (b) temperature (K) contours using equilibrium model (with volumetric condensation)

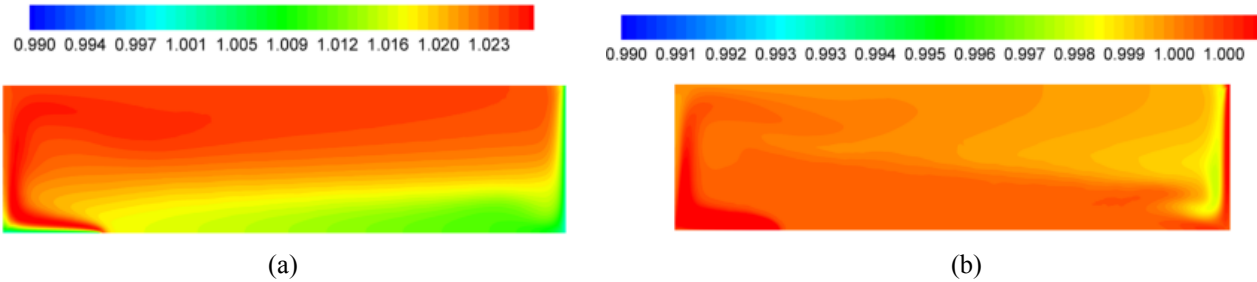


Fig. 7(a). Relative humidity contours using nonequilibrium model (without volumetric condensation) and (b) relative humidity contours using equilibrium model (with volumetric condensation)

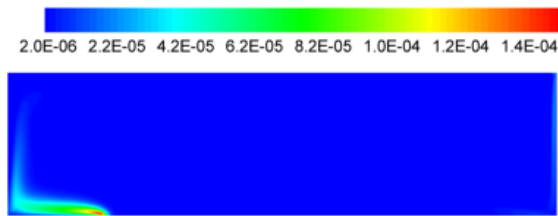


Fig. 8. Interphase mass transfer ($\text{kg}/\text{m}^2\text{-s}$) due to volumetric condensation using multiphase flow

equilibrium model as shown in Fig. 7(a). The mass transfer is expected to be maximum in regions where the degree of supersaturation is high because the rate is driven by the difference in local saturation levels.

IV. COMPARISON BETWEEN EXPERIMENTAL AND COMPUTED DATA

Figs. 9(a) and (b) show the comparison between experimentally obtained and computed condensation rates using the nonequilibrium and equilibrium models, respectively. Presented data are grouped together in four distinct sets that correspond to different convection regimes mentioned in Section II.B. Generally, both computed data sets have matched the trend of the experimental data, where the condensate rate increases with increased temperature difference. Though both models overpredict condensation rate, the equilibrium model matches the experimental data better, especially at lower temperature difference.

Figs. 10(a) and (b) show the temperature comparison at locations T3, T4, and T5 as indicated in Fig. 2. Only three sets of data are presented for clarity. The majority of temperature data have been underpredicted by the nonequilibrium model, whereas the match between the experimental and computed data is better for the equilibrium model. This is because the nonequilibrium model does not

consider volumetric phase change and does not account for the latent heat that is absorbed by the gas phase due to condensation. This added heat caused a higher temperature for the equilibrium model and brings it closer to experimental observation.

V. CONCLUSION

A combined experimental and computational study was conducted to understand the condensation-evaporation cycle in an enclosed space. Numerical techniques were adopted to model moisture redistribution and phase change for further application to study the cold trap process that has been tested and validated using the experimental data. Nonequilibrium and equilibrium multiphase models were developed and studied to explore the effect of volumetric condensation. Presented results showed the velocity, temperature, and relative humidity distribution of the system. Numerical results of the condensate rate and temperature matched the general trend and pattern observed in the experiment, but the equilibrium model provided a better prediction.

The numerical methodology presented here can be used to study a range of geophysical and engineering applications including cold-trap process, condenser behavior, and other waste disposal applications involving two-phase flows.

ACKNOWLEDGMENTS

The authors would like to acknowledge Steven Svedeman, Steven Green, and Don Bannon for their help in the design, fabrication, and performance of the test runs of the condensation cell.

This paper is an independent product of the Center for Nuclear Waste Regulatory Analyses and does not necessarily reflect the view or regulatory position of the U.S. Nuclear Regulatory

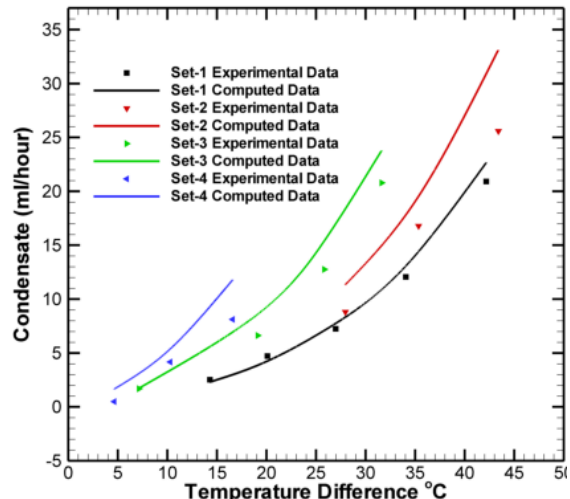
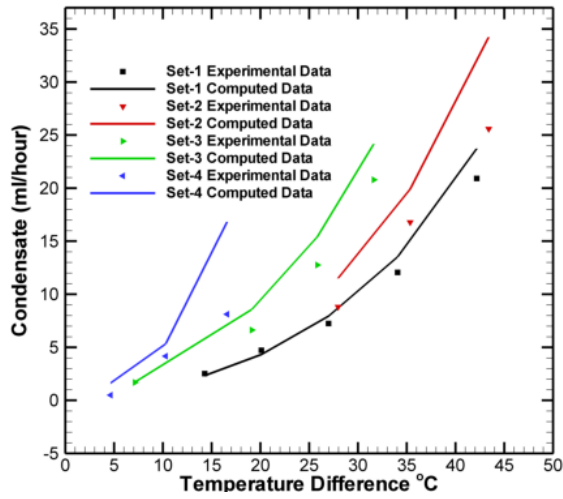


Fig. 9(a). Comparison of experimental and computed values of condensation rate using nonequilibrium model (without volumetric condensation) and (b) comparison of experimental and computed values of condensation rate using equilibrium model (with volumetric condensation)

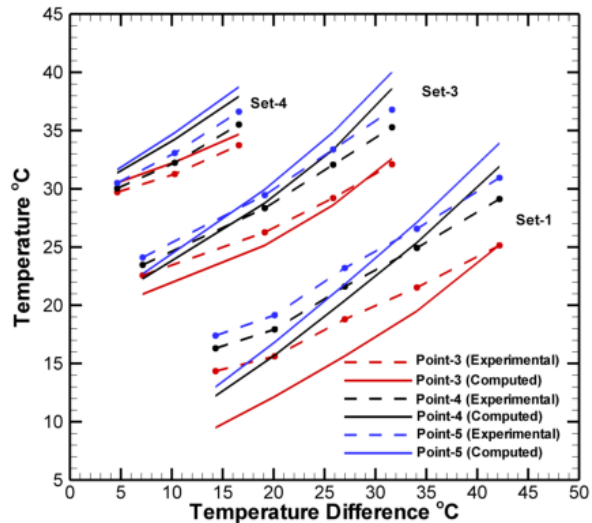
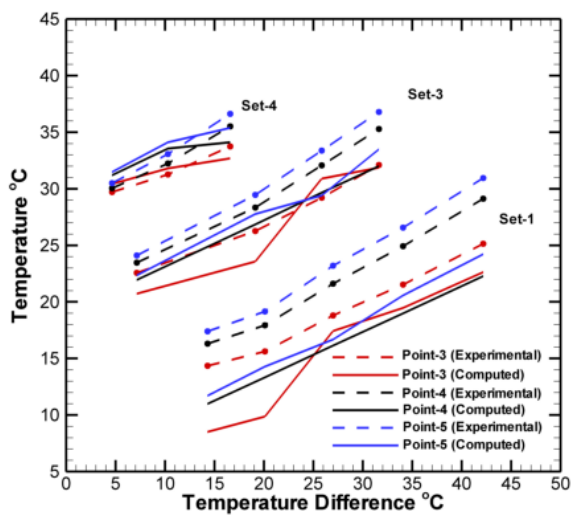


Fig. 10(a). Comparison of experimental and computed values of temperature using nonequilibrium model (without volumetric condensation) and (b) comparison of experimental and computed values of temperature using equilibrium model (with volumetric condensation)

Commission (USNRC). The USNRC staff views expressed herein are preliminary and do not constitute a final judgment or determination of the matters addressed or of the acceptability of any licensing action that may be under consideration at the USNRC.

REFERENCES

1. ANSYS-FLUENT "Version 12.1, User's Guide," ANSYS-Inc, Canonsburg, PA (2009).

2. J.P. VAN DOORMAL and G. D. RAITHBY, "Enhancements of the SIMPLE Method for Predicting Incompressible Fluid Flows," *Numerical Heat Transfer*, **7**, 147–163 (1984).
3. C. M. RHIE and W. L. CHOW, "Numerical Study of the Turbulent Flow Past an Airfoil With Trailing Edge Separation," *AIAA Journal*, **21**, 1523–1532 (1983).
4. F. R. MENTER, "Two-Equation Eddy-Viscosity Turbulence Models for Engineering Applications," *AIAA Journal*, **32**(8), 1598–1605

- (1994).
5. V. P. CAREY, "Liquid-Vapor Phase-Change Phenomena," Hemisphere Publishing Corporation, New York, NY, (1992). Second Edition (2007).
 6. H. C. KANG and M. H. KIM, "Characteristics of Film Condensation of Supersaturated Steam–Air Mixture on a Flat Plate," *International Journal of Multiphase Flow*, **25(8)**, 1601–1618 (1999).
 7. R. J. FOX, P. F. PETERSON, M. M. L. CORRADINI, and A. P. PERNSTEINER, "Free Convective Condensation in a Vertical Enclosure," *Nuclear Engineering and Design*, **177(1–3)**, pp. 71–89 (1997).
 8. H. J. H. BROUWERS and A. K. CHESTERS, "Film Models for Transport Phenomena With Fog Formation: The Classical Film Model," *International Journal of Heat and Mass Transfer*, **35**, 1–11 (1992).
 9. K. HIJIKATA and Y. MORI, "Forced Convective Heat Transfer of a Gas With Condensing Vapor Around a Flat Plate," *Heat Transfer Japanese Research*, **2**, pp. 81–101 (1973).

